Scale-Invariant Quantum Anomalous Hall Effect in Magnetic Topological Insulators beyond the Two-Dimensional Limit

Xufeng Kou,[1] Shih-Ting Guo,[2] Yabin Fan,[1] Lei Pan,[1] Murong Lang,[1] Ying Jiang,[3] Qiming Shao,[1] Tianxiao Nie,[1] Koichi Murata,[1] Jianshi Tang,[1] Yong Wang,[3] Liang He,[1] Ting-Kuo Lee,[2] Wei-Li Lee,[2,*] and Kang L. Wang[1,†]

[1]*Department of Electrical Engineering, University of California, Los Angeles, California 90095, USA*

[2]*Institute of Physics, Academia Sinica, Taipei 11529, Taiwan*

[3]*Center for Electron Microscopy and State Key Laboratory of Silicon Materials, Department of Materials Science and Engineering, Zhejiang University, Hangzhou 310027, China*

(Received 26 May 2014; revised manuscript received 28 July 2014; published 26 September 2014)

We investigate the quantum anomalous Hall effect (QAHE) and related chiral transport in the millimeter-size $(Cr_{0.12}Bi_{0.26}Sb_{0.62})_2Te_3$ films. With high sample quality and robust magnetism at low temperatures, the quantized Hall conductance of e^2/h is found to persist even when the film thickness is beyond the two-dimensional (2D) hybridization limit. Meanwhile, the Chern insulator-featured chiral edge conduction is manifested by the nonlocal transport measurements. In contrast to the 2D hybridized thin film, an additional weakly field-dependent longitudinal resistance is observed in the ten-quintuple-layer film, suggesting the influence of the film thickness on the dissipative edge channel in the QAHE regime. The extension of the QAHE into the three-dimensional thickness region addresses the universality of this quantum transport phenomenon and motivates the exploration of new QAHE phases with tunable Chern numbers. In addition, the observation of scale-invariant dissipationless chiral propagation on a macroscopic scale makes a major stride towards ideal low-power interconnect applications.

DOI: 10.1103/PhysRevLett.113.137201 PACS numbers: 75.47.−m, 73.43.Fj, 75.45.+j, 75.50.Pp

The discovery of the topological insulator (TI) has greatly broadened the landscape of condensed matter physics [1–3]. Owing to a nontrivial band topology and strong spin-orbit coupling in a three-dimensional (3D) TI material, gapless Dirac surface states protected by time-reversal symmetry (TRS) are formed, and the surface conductions exhibit an unusual spin-momentum locking feature [4–6]. In two-dimensional (2D) TIs, band inversion gives rise to counterpropagating helical edge channels with opposite spins, and elastic backscatterings from non-magnetic impurities are suppressed [7,8]. Accordingly, the resulting quantum spin Hall effect (QSHE) leads to a quantized longitudinal conductance of $2e^2/h$ in the absence of a magnetic field. However, since the dissipationless helical edge states are vulnerable to magnetic impurities and band potential fluctuations, TI materials with low defect density and high carrier mobility are crucial for the QSHE phase [9]. To date, the QSHE has been experimentally observed only in the 2D HgTe/CdTe [10,11] and InAs/GaSb quantum wells [12,13].

Alternatively, given the close connection between the intrinsic anomalous Hall effect and the quantum Hall effect (QHE) in terms of the band topology [14–16], it is expected that a 2D ferromagnetic (FM) insulator with a nonzero first Chern number (C_1) would give rise to the quantum anomalous Hall effect (QAHE) [14]. In such Chern insulators, the chiral edge states are formed due to the TRS breaking, and the spontaneous magnetization also localizes the dissipative states [17–19]. Among all possible candidates [20–24], it was proposed that, by adding appropriate exchange splitting into the QSHE system, one set of the spin subbands would remain in the inversion regime while the other became topologically trivial, therefore driving the 2D magnetic TI system into a QAHE insulator [25–27]. Moreover, it was found that, in magnetic tetradymite-type TI materials, robust out-of-plane magnetization could be developed directly from the large Van Vleck spin susceptibility in the host TI materials without the mediation of itinerant carriers [27–29]. By manipulating the Fermi level position and the magnetic doping, The QAHE in the 2D regime was recently observed in a five-quintuple-layer (QL) $Cr_{0.15}(Bi_{0.1}Sb_{0.9})_{1.85}Te_3$ film, where a plateau of Hall conductance σ_{xy} of e^2/h and a vanishing longitudinal conductance σ_{xx} were observed at 30 mK [30]. More generally, it has been suggested that the quantized Hall conductance could also be derived from the gapped top and bottom surfaces in 3D magnetic TI systems [7,31,32]. Furthermore, if the exchange field strength and film thickness were properly adjusted so that higher subbands would get involved in the band topology transition, a QAHE with a tunable Chern number could, in principle, be realized [33,34]. Nevertheless, the increased bulk conduction in the thicker films was detrimental and obscured the observation of the QAHE beyond the 2D hybridization thickness (>6 QL) [30]. As a result, the universality of the QAHE phase and its related quantum transport phenomena in the 3D regime still remain unexplored. Here, we report the observation of the QAHE in

$(Cr_{0.12}Bi_{0.26}Sb_{0.62})_2Te_3$ samples with a film thickness up to 10 QL. Given the chiral nature of the edge modes, we show that the quantization of the Hall conductance (e^2/h) persists in the device with millimeter-scale sizes. In contrast to the previous work [30], a nonzero longitudinal resistance is detected in our thick 10 QL sample and is found to be insensitive to external magnetic fields, indicating the possible presence of additional nonchiral side surface propagation modes. The corresponding nonlocal transport measurements further confirm the chiral property of a dissipationless QAHE state. This scale-invariant quantized chiral transport manifests the universality of the QAHE in both 2D and 3D thicknesses, and it may open up a practical route to construct new Chern insulators with higher Hall conductance plateaus [33–38].

To prepare the magnetic TI materials with pronounced FM orders and insulating bulk states, single-crystalline Cr-doped $(Bi_xSb_{1-x})_2Te_3$ films are grown by molecular beam epitaxy. Both the Cr doping level (12%) and the Bi/Sb ratio (0.3/0.7) are optimized so that the Fermi level positions of the as-grown samples are already close to the charge neutral point [29,39]. The growth is monitored by reflection high-energy electron diffraction (RHEED), and the film with a thickness of 10 QL is obtained after ten periods of RHEED oscillation, as shown in Fig. 1(b). In the meantime, high-resolution scanning transmission electron microscopy (HRSTEM) is used to characterize the film structure and crystalline configuration [40]. Figure 1(c) highlights the highly ordered hexagonal structure of the 10 QL $(Cr_{0.12}Bi_{0.26}Sb_{0.62})_2Te_3$ film with an atomically sharp interface on top of the GaAs substrate, and the uniform Cr distribution inside the host TI matrix is also confirmed by the energy dispersive x-ray (EDX) spectrum.

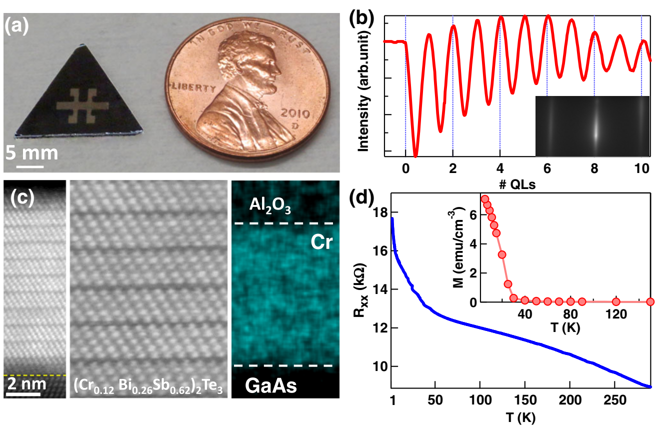

FIG. 1 (color online). Cr-doped $(Bi_xSb_{1-x})_2Te_3$ film structure and properties. (a) The image of the Hall bar structure with the dimension of 2 mm × 1 mm. (b) RHEED oscillation, showing that the grown Cr-doped $(Bi_xSb_{1-x})_2Te_3$ film has a thickness of 10 QL. Inset: RHEED pattern of the as-grown film. (c) Cross-sectional HRSTEM image, illustrating the crystalline structure of the 10 QL $(Cr_{0.12}Bi_{0.26}Sb_{0.62})_2Te_3$ film. The EDX mapping confirms that the Cr dopants distribute uniformly inside the TI layer. (d) Temperature-dependent resistance as the temperature drops from 300 to 1 K. Inset: Magnetic moment under field-cooled conditions. The applied field is 10 mT, and the Curie temperature is estimated to be $T_C = 30$ K.

To investigate the chiral transport properties in the QAHE regime, we deliberately fabricate the Hall bar devices with dimensions of 2 mm × 1 mm (i.e., 10 times larger than that used in Ref. [30]), as shown in Fig. 1(a). In the diffusive transport region ($T > 1$ K), the 10 QL $(Cr_{0.12}Bi_{0.26}Sb_{0.62})_2Te_3$ film shows a typical semiconductor behavior, where the sample resistance monotonically increases as the sample temperature drops from 300 to 1 K [Fig. 1(d)], indicating that the Fermi level is inside the bulk band gap [41]. Besides, the Curie temperature (T_C) is found to be around 30 K from the temperature-dependent magnetization under the field-cooled condition, as shown in the inset in Fig. 1(d) (Supplemental Material, Fig. S1 [42]).

Figures 2(a) and (b) show the magnetotransport results of the 10 QL $(Cr_{0.12}Bi_{0.26}Sb_{0.62})_2Te_3$ film. When $T < T_C$, the Hall resistance $R_{xy} = R_{14,62}$ in Fig. 2(a) develops a square-shaped hysteresis loop, indicating the robust FM order with an out-of-plane magnetic anisotropy, and the butterfly-shaped double-split longitudinal resistance $R_{xx} = R_{14,65}$ is also observed in Fig. 2(b) [28,29]. Our 10 QL $(Cr_{0.12}Bi_{0.26}Sb_{0.62})_2Te_3$ film reaches the QAHE regime when the sample temperature falls below 85 mK. As demonstrated in Figs. 2(a) and 2(b), the R_{xy} reaches the

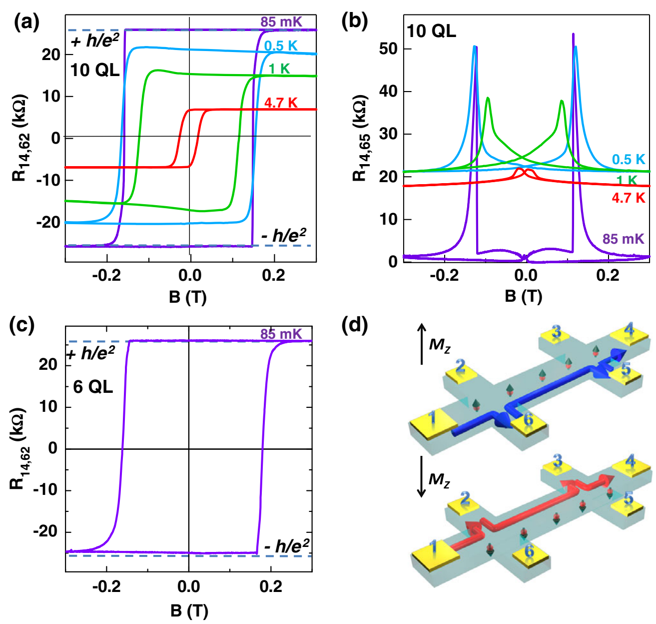

FIG. 2 (color online). The QAHE in the $(Cr_{0.12}Bi_{0.26}Sb_{0.62})_2Te_3$ thin films. (a) Hysteresis $R_{xy} - B$ curves of the 10 QL film at different temperatures. For $T < 85$ mK, R_{xy} attains the quantized value of h/e^2. (b) Butterfly-shaped $R_{xx} - B$ curves of the 10 QL film. In the QAHE regime, R_{xx} nearly vanishes at low fields. (c) The QAHE is also observed in the 6 QL film at a similar temperature of 85 mK. (d) Schematics of the chiral edge conduction in the QAHE regime. The current flows from the first contact to the fourth contact, and the magnetization of the Cr-doped TI film is along the z direction.

quantized value of h/e^2 (25.8 kΩ) at $B = 0$ T while R_{xx} has nearly vanished. Meanwhile, it is important to highlight that the QAHE is also realized in the 6 QL $(Cr_{0.12}Bi_{0.26}Sb_{0.62})_2Te_3$ film with a similar phase transition temperature of 85 mK, as shown in Fig. 2(c) [42]. Therefore, the thickness-dependent results provide strong evidence that the stability of the QAHE phase in magnetic TIs is maintained as the film thickness varies across the hybridization limit (whereas in the QHE regime, the formation of the precise Landau level quantization requires the electrons to be strictly confined in the 2D region [45]).

To quantitatively understand the chiral edge transport in our samples, we thus apply the Landauer-Büttiker formalism that [46]

$$I_i = \frac{e^2}{h}\sum_j (T_{ji}V_i - T_{ij}V_j), \tag{1}$$

where I_i is the current flowing from the ith contact into the sample for single spin, V_i is the voltage on the ith contact, and T_{ji} is the transmission probability from the ith to the jth contacts [47,48]. In our six-terminal Hall bar structure shown in Fig. 2(d), the voltage is applied between the first and fourth contacts ($V_1 = V$, $V_4 = 0$), and the other four contacts are used as the voltage probes ($I_2 = I_3 = I_5 = I_6 = 0$). In the QAHE regime, since the TRS is broken, electrons can flow only one way along the edge channel with the conduction direction determined by the magnetization orientation [49]. Specifically, when the film is magnetized along the $+z$ direction [upper panel of Fig. 2(d)], the nonzero transmission matrix elements for the QAHE state are $T_{61} = T_{56} = T_{45} = 1$ [11,49], and the corresponding voltage distributions are given by $V_6 = V_5 = V_1 = (h/e^2)I$ and $V_2 = V_3 = V_4 = 0$. On the other hand, when the magnetization reverses its direction [lower panel of Fig. 2(d)], the edge current flows through the second and third contacts, thus making $V_2 = V_3 = V_1 = (h/e^2)I$ and $V_5 = V_6 = V_4 = 0$. Consequently, $R_{14,62} = (V_6 - V_2)/I$ is positive for the $M_Z > 0$ case and changes to a negative sign if $M_Z < 0$. Simultaneously, except for the sharp magnetoresistance (MR) peaks at the coercivity fields, the vanishing $R_{12,65}$ in the fully magnetized region is also anticipated from Eq. (1), since the presence of the dissipationless chiral edge states leads to zero voltage drop along the edge channel. Accordingly, the consistency between the scenario described by Eq. (1) and the experimental observations in Fig. 2 clearly reveals the chiral edge transport nature of QAHE.

Compared with the QSHE helical states which were observed in only micrometer-scale devices [10–12], the observation of a scale-invariant QAHE with perfect quantization on the macroscopic scale is significant. Based on Eq. (1), the chiral nature in the QAHE regime causes $(T_{i,i+1}, T_{i+1,i}) = (0, 1)$. In other words, once the magnetization is fixed, backward conduction is always prohibited by the chirality, and hence the decoherence process from the lateral contacts cannot lead to momentum and energy relaxation [11,49]. Together with the thickness-dependent results, we may conclude that when appropriate spin-orbit interaction and perpendicular FM exchange strength are present in a bulk insulating magnetic TI film where the Fermi level resides inside the surface gap [26,27,33], the QAHE resistance is always quantized to be h/e^2, regardless of the device dimensions and dephasing process (Supplemental Material, Figs. S4 and S5 [42]).

Figure 3(a) shows the $R_{xx} - T$ and $R_{xy} - T$ results of the 10 QL $(Cr_{0.12}Bi_{0.26}Sb_{0.62})_2Te_3$ film at $B = 3$ and 15 T in the low-temperature region ($T < 1$ K). Both the enhanced magnetization and the reduced thermal activations at lower temperatures help localize the bulk conduction channels and thus drive the system from the regular diffusive transport regime ($T > 1$ K) towards the chiral edge conduction regime. As a result, R_{xx} diminishes rapidly as the sample temperature drops, which is opposite to the $R_{xx} - T$ relation in the high-temperature region as shown in Fig. 1(d). Moreover, when the magnetic TI film reaches the QAHE state below 85 mK, we also observe a nonzero R_{xx} similar to the previously reported 5 QL $Cr_{0.15}(Bi_{0.1}Sb_{0.9})_{1.85}Te_3$ film case [30]. It is noted that the underlying mechanisms of the nonzero longitudinal resistances in these two systems are quite different. In particular, it was reported that, when a large external magnetic field ($B > 10$ T) was applied, the 5 QL film was driven into a perfect QHE regime, and R_{xx} diminished almost to zero [30]. In contrast, it is apparent from Fig. 3(a) that the longitudinal resistance in our 10 QL $(Cr_{0.12}Bi_{0.26}Sb_{0.62})_2Te_3$ sample remains at 3 kΩ even when the applied magnetic field reaches 15 T. More importantly, unlike the bulk conduction case which has a typical parabolic MR relation [50], R_{xx} at $T = 85$ mK exhibits little field dependence when the magnetic field is larger than 3 T [Fig. 3(b)]. Consequently, it may be suggested that the nonzero R_{xx} in the thicker 10 QL magnetic TI film is more likely associated with a unique dissipative edge conduction, whose origins cannot be simply attributed to either the variable range hopping [30] or the gapless

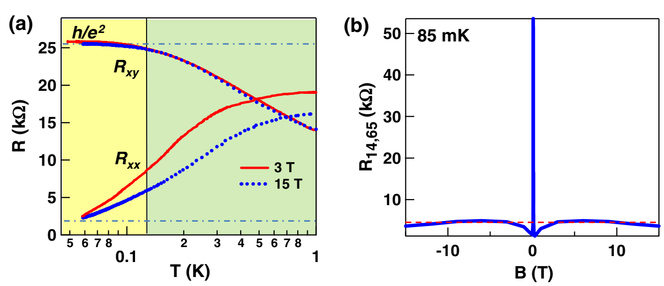

FIG. 3 (color online). Nonzero longitudinal resistance in the QAHE regime. (a) Temperature-dependent R_{xx} and R_{xy} of the 10 QL $(Cr_{0.12}Bi_{0.26}Sb_{0.62})_2Te_3$ film at $B = 3$ and 15 T in the low-temperature region. (b) Magnetic field dependence of R_{xx} at 85 mK. R_{xx} in our 10 QL magnetic TI sample shows little field dependence when $B > 3$ T.

quasihelical edge states [49] as proposed for the 5 QL magnetic TI film.

To further confirm the presence of the dissipative edge conduction to the QAHE state, we perform nonlocal measurements on the six-terminal Hall bar device under different magnetic fields in Fig. 4 [49]. Two different nonlocal configurations are investigated: in case A, the current is passed through contacts 1 (source) and 2 (drain) while the nonlocal resistance between contacts 5 and 4 ($R_{12,54}$) is measured [top inset of Fig. 4(a)]; in case B, a quasi-H-bar geometry is adopted such that contacts 2 and 6 are designated as the source or drain pads while contacts 3 and 5 are used as the voltage probes [$R_{26,35}$, top inset of Fig. 4(b)] [49]. In the QAHE regime ($T < 85$ mK), it can be clearly seen that both $R_{12,54}$ and $R_{26,35}$ display square-shaped hysteresis windows, but their polarities are opposite. In other words, when $B < -0.2$ T, $R_{12,54}$ reaches the high-resistance state of 15Ω while $R_{26,35}$ is at the low-resistance state close to zero. Here, we point out that the nonlocal resistances can be understood from the chirality of the QAHE. In the inset of the bottom Fig. 4(a), for example, we show that, when the film is magnetized along the $+z$ direction, the chirality forces the QAHE dissipationless current flow from contact 1 to contact 2 through the $1 \rightarrow 6 \rightarrow 5 \rightarrow 4 \rightarrow 3 \rightarrow 2$ contacts successively and, in turn, "shorts" the contacts so that $V_6 = V_5 = V_4 = V_3 \sim V_1 = V$ [46]. As a result, the voltage drop between these contacts is negligible, and $R_{12,54}$ is driven into the low-resistance state (2Ω). On the other hand, when the magnetization is reversed ($-z$ direction), the first and second contacts are directly connected through the upper edge [lower left panel of Fig. 4(a)], and the voltage probes from V_3 to V_6 are now away from the QAHE channel. Consequently, the nonlocal signal relates only to the voltage drop caused by the dissipative edge channel, which gives rise to a larger value of $R_{12,54}$. The same transport principle can also be applied to the quasi-H-bar nonlocal configuration (case B), and the illustrations of field-dependent conduction paths are consistent with the measured $R_{26,35}$ results, as shown in the bottom panels of Fig. 4(b) (Supplemental Material, Fig. S6 [42]). It is noted that, in contrast to the QAHE regime ($T < 85$ mK), both $R_{12,54}$ and $R_{26,35}$ are dominated by the larger bulk conduction component at a higher temperature of 4.7 K (i.e., the nonlocal resistances are more than 10 times larger than those probed at 85 mK). In such a diffusive transport regime, the square-shaped hysteresis nonlocal signals are replaced by the ordinary parabolic MR backgrounds, and the polarity differences between $R_{12,54}$ and $R_{26,35}$ also disappear. In summary, both the field-independent R_{xx} shown in Fig. 3(b) and the nonlocal resistances displayed in Fig. 4 confirm the coexistence of a QAHE chiral edge channel and the additional dissipative edge conduction in the thick 10 QL Cr-doped TI sample.

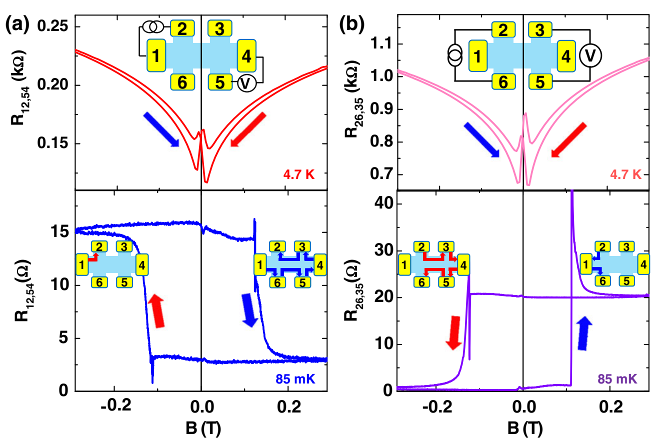

FIG. 4 (color online). Nonlocal measurements of the six-terminal Hall bar device. (a) Case A: The current is applied through the first to the second contact, and the nonlocal voltages are measured between the fourth and fifth contacts at $T = 85$ mK and 4.7 K. (b) Case B: The current is applied through the second to the sixth contact, and the nonlocal voltages are measured between the third and fifth contacts with different magnetizations. Inset: Illustrations of the QAHE channel under different magnetizations. The red solid arrow indicates that the magnetic field is swept from positive ($+z$) to negative ($-z$), whereas the blue solid arrow corresponds to the opposite magnetic field sweeping direction.

In a uniformly doped 3D magnetic TI, the out-of-plane magnetization along the z direction opens gaps on the top and bottom surfaces [7,21,31,32]. Meanwhile, the gapless Dirac point on the side surfaces is shifted away from the symmetric point (Γ) (Supplemental Material, Fig. S7 [42]). Under such circumstances, the backscattering may not be suppressed anymore, and the side surface conduction thus would become dissipative [31], which is intimately related to the dissipative edge channel unveiled in Figs. 3 and 4. Nevertheless, further investigations are needed to elucidate the intrinsic mechanisms of the dissipative edge states in the 3D magnetic TI system. Systematic thickness-dependent experiments as well as relevant theoretical modeling are required to address this issue in more detail. In addition, more careful design on the contact geometry is also needed in order to reveal the proposed half-quantized Hall conductance from a single top (bottom) surface edge [7,31].

In conclusion, our results demonstrate the QAHE in magnetic TI material with a thickness beyond the 2D hybridization limit. Both the scale-invariant dissipationless Hall conductance and two-state nonlocal resistances not only reflect the chiral transport character of the QAHE state, but also reveal the distinctions between the QAHE and the other two quantum phases (i.e., QHE and QSHE). Moreover, a dissipative channel is observed for the thick 10 QL magnetic TI sample, and its origin is different from the 2D hybridization thickness case. The scale-invariant feature of the QAHE may motivate the exploration of new QAHE phases and may provide novel chiral interconnects with higher quantized conduction channels.

X. K., S.-T. G., and Y. F. contributed equally to this work.

We thank Dr. J. Wang, Professor X. L. Qi, Professor D. Goldhabor-Gordon, Professor Y. Tserkovnyak, and Professor Y. G. Yao for helpful discussions. We are grateful for the support from the DARPA Meso program under Contracts No. N66001-12-1-4034 and No. N66001-11-1-4105. We also acknowledge support from the FAME Center, one of six centers of STARnet, a Semiconductor Research Corporation program sponsored by MARCO and DARPA. K. L. W. acknowledges the support of the Raytheon endorsement. X. K. and M. L. acknowledge partial support from the Qualcomm Innovation Fellowship. W. L. L. acknowledges funding support from the Academia Sinica 2012 Career Development Award in Taiwan. Y. W. acknowledges support from National Natural Science Foundation of China (No. 11174244 and No. 51390474), Zhejiang Provincial Natural Science Foundation (LR12A04002), and National 973 Project of China (No. 2013CB934600).

Note added.—Recently, we became aware of a related work by Checkelsky *et al.* [51] that reports the observation of the QAHE in a 8 QL Cr-doped magnetic TI.

---

*Corresponding author.
wlee@phys.sinica.edu.tw
†Corresponding author.
wang@seas.ucla.edu

[1] J. E. Moore, Nature (London) **464**, 194 (2010).
[2] B. A. Bernevig, T. L. Hughes, and S. C. Zhang, Science **314**, 1757 (2006).
[3] C. L. Kane and E. J. Mele, Phys. Rev. Lett. **95**, 146802 (2005).
[4] X. L. Qi and S. C. Zhang, Phys. Today **63**, No. 1, 33 (2010).
[5] M. Z. Hasan and C. L. Kane, Rev. Mod. Phys. **82**, 3045 (2010).
[6] D. Hsieh *et al.*, Nature (London) **460**, 1101 (2009).
[7] X. L. Qi, T. L. Hughes, and S. C. Zhang, Phys. Rev. B **78**, 195424 (2008).
[8] Y. Zhang *et al.*, Nat. Phys. **6**, 584 (2010).
[9] S. Oh, Science **340**, 153 (2013).
[10] M. Konig, S. Wiedmann, C. Brune, A. Roth, H. Buhmann, L. W. Molenkamp, X.-L. Qi, and S.-C. Zhang, Science **318**, 766 (2007).
[11] A. Roth, C. Brune, H. Buhmann, L. W. Molenkamp, J. Maciejko, X.-L. Qi, and S.-C. Zhang, Science **325**, 294 (2009).
[12] I. Knez, R. R. Du, and G. Sullivan, Phys. Rev. Lett. **107**, 136603 (2011).
[13] L. J. Du *et al.*, arXiv:1306.1925.
[14] N. Nagaosa, J. Sinova, S. Onoda, A. H. MacDonald, and N. P. Ong, Rev. Mod. Phys. **82**, 1539 (2010).
[15] D. J. Thouless, M. Kohmoto, M. P. Nightingale, and M. den Nijs, Phys. Rev. Lett. **49**, 405 (1982).
[16] F. D. M. Haldane, Phys. Rev. Lett. **93**, 206602 (2004).
[17] T. Dittrich, *Quantum Transport and Dissipation* (Wiley-VCH, New York, 1998).
[18] S. R. E. Yang, A. H. Macdonald, and B. Huckestein, Phys. Rev. Lett. **74**, 3229 (1995).
[19] H. Z. Lu, J. R. Shi, and S. Q. Shen, Phys. Rev. Lett. **107**, 076801 (2011).
[20] F. D. M. Haldane, Phys. Rev. Lett. **61**, 2015 (1988).
[21] K. Nomura and N. Nagaosa, Phys. Rev. Lett. **106**, 166802 (2011).
[22] M. Onoda and N. Nagaosa, Phys. Rev. Lett. **90**, 206601 (2003).
[23] Z. H. Qiao, S. A. Yang, W. Feng, W.-K. Tse, J. Ding, Y. Yao, J. Wang, and Q. Niu, Phys. Rev. B **82**, 161414 (2010).
[24] F. Guinea, M. I. Katsnelson, and A. K. Geim, Nat. Phys. **6**, 30 (2010).
[25] C. X. Liu, X. L. Qi, X. Dai, Z. Fang, and S. C. Zhang, Phys. Rev. Lett. **101**, 146802 (2008).
[26] H. Jin, J. Im, and A. J. Freeman, Phys. Rev. B **84**, 134408 (2011).
[27] R. Yu, W. Zhang, H.-J. Zhang, S.-C. Zhang, X. Dai, and Z. Fang, Science **329**, 61 (2010).
[28] C. Z. Chang *et al.*, Adv. Mater. **25**, 1065 (2013).
[29] X. F. Kou *et al.*, ACS Nano **7**, 9205 (2013).
[30] C.-Z. Chang *et al.*, Science **340**, 167 (2013).
[31] R. L. Chu, J. R. Shi, and S. Q. Shen, Phys. Rev. B **84**, 085312 (2011).
[32] K. He, X.-C. Ma, X. Chen, L. Lu, Y.-Y. Wang, and Q.-K. Xue, Chin. Phys. B **22**, 067305 (2013).
[33] J. Wang, B. Lian, H. Zhang, Y. Xu, and S. C. Zhang, Phys. Rev. Lett. **111**, 136801 (2013).
[34] H. Jiang, Z. Qiao, H. Liu, and Q. Niu, Phys. Rev. B **85**, 045445 (2012).
[35] S. Murakami, N. Nagaosa, and S. C. Zhang, Science **301**, 1348 (2003).
[36] B. A. Bernevig and S. Zhang, IBM J. Res. Dev. **50**, 141 (2006).
[37] X. Zhang and S. C. Zhang, Proc. SPIE Int. Soc. Opt. Eng. **8373**, 837309 (2012).
[38] Y. P. Chen, Proc. SPIE Int. Soc. Opt. Eng. **8373**, 83730B (2012).
[39] X. F. Kou *et al.*, Nano Lett. **13**, 4587 (2013).
[40] Y. Jiang, Y. Wang, J. Sagendorf, D. West, X. Kou, X. Wei, L. He, K. L. Wang, S. Zhang, and Z. Zhang, Nano Lett. **13**, 2851 (2013).
[41] X. F. Kou *et al.*, J. Appl. Phys. **112**, 063912 (2012).
[42] See Supplemental Material at http://link.aps.org/supplemental/10.1103/PhysRevLett.113.137201 for detailed discussions on both magnetotransport and nonlocal measurements, more QAHE results on different samples, and other supporting data. The Supplemental Material includes Refs. [43–44].
[43] L. Berger, Phys. Rev. B **2**, 4559 (1970).
[44] A. Fert, J. Phys. F **3**, 2126 (1973).
[45] M. Stone, *Quantum Hall Effect* (World Scientific, Singapore, 1992).
[46] S. Datta, *Electronic Transport in Mesoscopic Systems* (Cambridge University Press, Cambridge, England, 1997).
[47] M. Buttiker, Phys. Rev. Lett. **57**, 1761 (1986).
[48] M. Buttiker, Phys. Rev. B **38**, 9375 (1988).
[49] J. Wang, B. Lian, H. Zhang, and S. C. Zhang, Phys. Rev. Lett. **111**, 086803 (2013).
[50] M. H. Liu *et al.*, Phys. Rev. Lett. **108**, 036805 (2012).
[51] J. G. Checkelsky *et al.*, Nat. Phys. (to be published).